Journal of the American Heart Association

ORIGINAL RESEARCH

NLRP3 Inflammasome Activation in Peripheral Arterial Disease

Francesca Bartoli-Leonard, PhD; Jonas Zimmer; Abhijeet R. Sonawane, PhD; Katelyn Perez, BS; Mandy E. Turner, PhD; Shiori Kuraoka, PhD; Tan Pham, BS; Feifei Li, MD, PhD; Masanori Aikawa, MD, PhD; Sasha Singh, PhD; Luke Brewster, MD, PhD; Elena Aikawa, MD, PhD

BACKGROUND: Peripheral arterial disease (PAD) is estimated to affect 7% of the adult population in the United States; however, there is currently little understanding of the key cellular and molecular pathways at play. With PAD characterized by vascular inflammation and associated calcification, the current study set out to elucidate the role of NLRP3 (nucleotide oligomerization domain-like receptor family, pyrin domain containing 3) inflammasome activation in the current cohort.

METHODS AND RESULTS: Global proteomics of human vessels with and without PAD from a total of 14 donors revealed an increase of proinflammatory associated ontologies, specifically acute phase and innate immunity. Targeted mass spectrometry showed a significant increase in NLRP3, confirmed by NLRP3 ELISA. Histological analysis from the same patients demonstrated expression of NLRP3, colocalizing in immunoreactive CD68 (cluster of differentiation 68) and CD209 (cluster of differentiation 209) macrophages. Moreover, transmission electron microscopy showed the locality of macrophage-like cells in the presence of calcification, with confocal microscopy further validating the localization of CD68, NLRP3, and calcification via near-infrared calcium tracer. Systemic inflammation and the presence of the NLRP3 inflammasome was assessed via flow cytometry and ELISA, respectively. Compared with patients without PAD, NLRP3 expression was significantly increased in serum. In addition, proinflammatory cytokine presence was significantly increased in disease versus control, with IL (interleukin)-1β, TNF-α (tumor necrosis factor α), and IL-33 demonstrating the greatest disparity, correlating with NLRP3 activation.

CONCLUSIONS: The current findings demonstrate a link between NLRP3, macrophage accumulation, and calcification in arteries of patients with PAD, suggesting an association or possible driver of PAD in these patients.

Key Words: peripheral ■ proteomics ■ vascular biology ■ vascular disease ■ vascular disease inflammation

Peripheral arterial disease (PAD) is characterized by stenosis or occlusion in vessels between the aortoiliac and the pedal arteries, with 90% of PAD affecting the lower extremities. In the United States, 8.5 million people are diagnosed with PAD; however, with only 50% of PAD cases symptomatic, the true incidence may be much higher.[1] Classical cardiovascular risk factors such as smoking, diabetes, hypercholesteremia, and hypertension play a major role in the initiation and progression of PAD; however, the prognostic potency of these covariates is not unanimously agreed on and further stratification of risk factors is required to standardize the field.[2,3] Notably, of the 100 000 limb amputations performed each year in the United States, more than half of these can be contributed to PAD, underscoring the desperate need for greater understanding of the molecular mechanisms at play.[4]

Although PAD can be diagnosed via noninvasive methods such as Doppler ultrasound or systolic blood pressure ratios to calculate the ankle–brachial index, there is currently no specific pharmacological treatment for PAD available. Patients are often prescribed

Correspondence to: Elena Aikawa, MD, PhD, Brigham and Women's Hospital, Harvard Medical School, 3 Blackfan Street, 17th Floor, Boston, MA 02115. Email: eaikawa@bwh.harvard.edu

Supplemental Material is available at https://www.ahajournals.org/doi/suppl/10.1161/JAHA.122.026945

For Sources of Funding and Disclosures, see page 8.

JAHA is available at: www.ahajournals.org/journal/jaha

CLINICAL PERSPECTIVE

What Is New?

- This is the first global proteomic screen of peripheral arterial disease (PAD) patient vessels, demonstrating the unique inflammatory cascades present within these patients.
- Targeted proteomics and patient plasma screening identified active NLRP3 and its downstream effectors within PAD, which was lower within non-diseased vasculature.

What Are the Clinical Implications?

- With the incidence of PAD >230 million adults worldwide currently and treatment approaches focused on surgical intervention, understanding the mechanisms present in PAD will allow for targeted pharmacological intervention to reduce the global pathological burden.
- Given that PAD is associated with the increased risk of cardiac comorbidity and cardiac and cerebrovascular ischemic events, further studies are now needed to determine the clinical implication of pharmacologically reducing vascular inflammation in this cohort before surgical intervention.

Nonstandard Abbreviation and Acronym

NLRP3	nucleotide oligomerization domain-like receptor family, pyrin domain containing 3

a multitude of medications (including but not limited to antidiabetics, antihypertensives, antiplatelets, anticoagulants, PCSK9 [proprotein convertase subtilisin/kexin type 9] inhibitors, and statins) to manage the classical cardiovascular risk factors, which do not directly address the inflammatory disease risk[1] but do reduce the risk of overall cardiovascular outcomes.[5] Although inflammation has been demonstrated to be important for the initiation and progression of atherosclerosis, there has been poor consensus about the key players in the inflammatory cascades in PAD, with the majority of previous studies focusing on clinical imaging and the utility of current pharmacotherapeutics. Although there are several candidate inflammatory triggers, such as the aforementioned traditional proatherogenic risk factors, no inflammatory mechanism beyond oxidative stress and IL (interleukin)-1β[5] has been shown to be directly linked to promoting inflammation in PAD.

Currently one of the strongest candidates in inflammatory-driven PAD is angiotensin II signaling and the related production of reactive oxygen species as a result of its association with hypertension,[6] and 80% of patients with PAD are diagnosed with hypertension.[2,7] Thus, a multitude of clinical trials have been conducted or are underway (NCT001684678, NCT00681226, NCT00720577, NCT03240068) seeking to address the inflammatory mechanisms at play. Reactive oxygen species and its associated proinflammatory cytokines IL-6 and Monocyte Chemoattractant Protein-1 have been shown to positively regulate NLRP3 (nucleotide oligomerization domain-like receptor family, pyrin domain containing 3) inflammasome activity in macrophages in patients with aneurysms,[8] which promotes a proinflammatory and procalcific environment in the vasculature.[6] An important part of innate immunity, the NLRP3 inflammasome participates in the clearance of pathogens and the promotion of a proinflammatory macrophage phenotype, which have been demonstrated to play critical roles in the immune microenvironment of atherosclerosis.[9] However, the presence of both macrophages and NLRP3 inflammasome in PAD requires further investigation. Thus, the current study aimed to investigate the presence of the NLRP3 inflammasome and associated macrophage infiltration and proinflammatory cytokines to PAD.

METHODS

Data are available from the corresponding author on request. All reagents were purchased from Sigma unless stated otherwise. Detailed methods are available in Data S1.

Sample Collection and Histological Analysis

Human peripheral arteries were harvested from patients undergoing limb amputation following informed consent, and all procedures were conducted in accordance with the Declaration of Helsinki following Emory institutional review board protocol approval. Tissue samples were snap frozen on harvesting (Table S1). Serum samples were collected from patients with PAD before surgery (Table S2). Control blood was purchased from 6 donors (Research Blood Components). On arrival, samples were dissected on ice, with half retained for proteomics analysis and the other embedded in OCT freezing medium and frozen. Histological sections were stained with Oil Red O and Alizarin Red to assess lipid and calcium deposition, respectively. CD68, CD209, NLRP3, IL-1β, and caspase-1 were assessed via immunohistochemistry. Colocalization of calcification, NLPR3, and CD68 was assessed via confocal microscopy (Table S3).

Transmission Electron Microscopy

Fresh frozen sections were cut at 20-uM sections and placed in 4% paraformaldehyde with 0.1% glutaraldehyde for 2 hours before placing in PBS supplemented

with 20 mM glycine and delivered to the Harvard Medical School Electron Microscopy Facility. Samples were then infiltrated with 2.3 M sucrose in PBS for 15 minutes and cut onto carbon-coated copper grids before imaging by the core on an AMT camera system, HV=80.0 kV, cal=0.002 micron/pix.

NLRP3 ELISA

Human NLRP3 SimpleStep ELISA (ab27401, Abcam) was run following the manufacturer's instructions.

Proteomic Analysis

Samples were homogenized using Precellys tissue homogenizer (Precelly), and the supernatant was digested using iST in a solution-digestion kit (PreOmics) as per the manufacturer's instructions. Data-dependent acquisition mass spectrometry was acquired on the Orbitrap fusion Lumos, and spectra was queried against the human UniProt database. Targeted mass spectrometry was conducted against NLRP3, with quantification of each fragment ion's monoisotopic peak quantified using QualBrowser (Thermo Fisher Scientific) (Table S4). Differentially abundant proteins between PAD and control were identified using limma 3.46.[10] The differential abundant proteins list was then analyzed for enriched pathways using clusterProfiler 3.18[11] in R using the function enrichGO. The ontologies were plotted using cnetplot().

Multianalyte LegendPlex Flow Assay

Human inflammation panel 1 and a custom LegendPlex panel (containing IL-6, IL-18, IL-9, and IL-1β) (Cat. 740809 and 900001042, BioLegend) was conducted following the manufacturer's instructions.

Statistical Analysis

GraphPad Prism (version 9.0) and R (version 4.2) were used to analyze data. Nonparametric tests such as the Wilcoxon test were conducted on non-normally distributed data. Association of NLRP3 and cytokines was conducted via linear regression on GraphPad Prism. Graphs were produced in Prism and R. Proteomic data exploration was conducted using Qlucore Omics Explorer 3.2 (Qlucore).

RESULTS

Whole-Tissue Proteomics Identifies Inflammatory and Immune Response Proteins in PAD

Although previous PAD studies have focused on the clinical implications of disease progression, little is known about the molecular mechanisms of PAD. Thus, this study sought to assess the unique proteomic signature in patients with PAD. Label-free liquid chromatography mass spectrometry on fresh-frozen human peripheral arteries from patients undergoing limb amputation with and without diagnosed PAD (n=10 and n=4, respectively) was performed (Table S1).

Whole tissue proteomics identified 2115 unique proteins (≥2 unique-peptide filters), and there was near complete overlap (97%): 2049 proteins, 58 unique to the control tissue and 8 to the disease (Figure 1A). Principal component analysis further revealed clear disease specific variance between control and disease patient cohorts, with no statistical filtering (Figure 1B). A heatmap of differential abundance analysis in the cohort highlighted the differences between disease versus control conditions, with 158 differentially enriched proteins increased in the PAD and 30 enriched in control tissue (Figure 1C) (false discovery rate<0.05, abs[log fold-change]>2), highlighting the subtle yet notable differences in protein abundance, which may impact PAD. Further investigation of ontology enrichment analysis (Table S1–S5) into significantly differentially expressed proteins identified gene ontologies of proteins with decreased abundance in PAD related to extracellular matrix assembly, organization, and structure (MYH11, NAXD, EXOC8, COL4A2, FMOD, COL1A2, COLGALT1, VWA1, COL3A1, GAS6, LAMB2, LAMA5, COL8A1) (Figure 1D). Proteins with increased expression in PAD highlighted gene ontology enrichment such as humoral immune response (IGLC2, CPN1, CHGA, IGHD, IGHVs), acute inflammatory response (SERPINF2, APOL2, CD163, ORM), and compliment activation (IGHD, CPN1, CFHR1, FGR2B, APOA2) (Figure 1E). As a result of the association between enriched proinflammatory pathways and inflammasome involvement in the pathogenesis of atherosclerotic-related diseases,[6] the presence of the inflammasome in whole tissue was assessed via ELISA (Figure 1F). NLRP3 protein was significantly increased in PAD compared with control vessels (P=0.0360). Furthermore, targeted mass spectrometry was conducted to assess the NLRP3 inflammasome expression in the vessels. One peptide in the HD1 domain corresponding to 3 fragment ions was quantified (Figure 1G, Table S4), demonstrating a significant increase in NLPR3 peptide fragments in PAD over control vessels (P=0.0130). This result, coupled with the ELISA, suggests an increase NLRP3 inflammasome presence unique to patients with PAD.

Histological Analysis of PAD Vessels Identifies CD68-Positive Inflammasome-Activated Cells

Histological analysis was undertaken to assess the localization and presence of proinflammatory responses

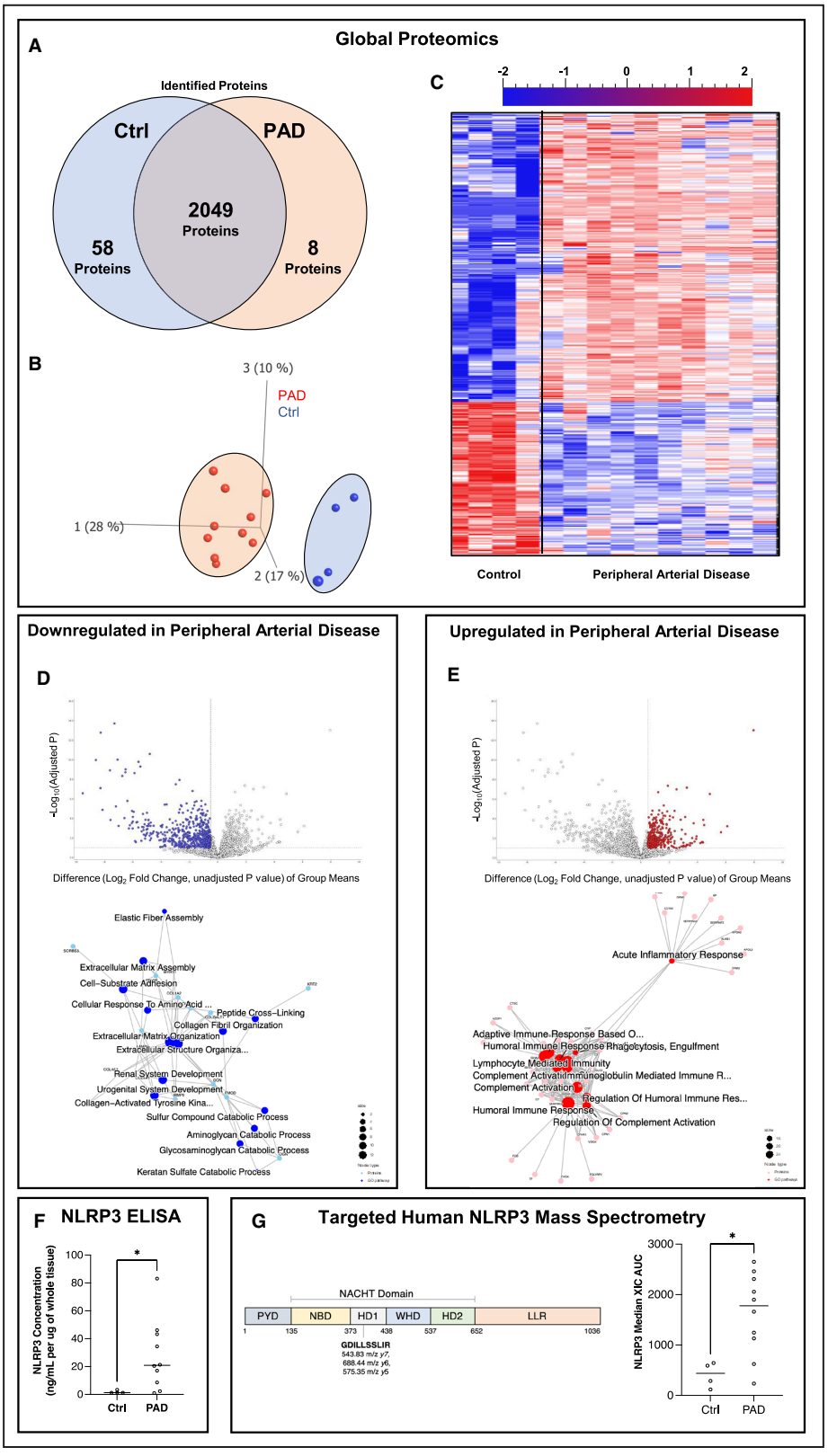

implicated by the proteomics as well as NLRP3 inflammasome markers in diseased vessels. Hematoxylin–eosin and Alizarin Red staining (Figure 2A and 2B) demonstrated the increased infiltration of cellular bodies in the vessel wall in diseased compared with control sections. Although moderate calcification was seen in both tissues, concentric, medial calcification was visible in the PAD tissue, with smaller,

Figure 1. Proteomic analysis of PAD highlights proinflammatory networks.
A, Whole tissue proteomic analysis following median peptide normalization with unique 2-peptide filter, and 97% of quantified proteins overlap. **B**, Unfiltered principal component analysis plot of proteomic analysis demonstrates disease-specific sample clustering. **C**, Hierarchical clustered heatmap ($q \leq 0.05$, fold change >1) shows 2-way comparison of disease vs control proteomics. **D** and **E**, Volcano plots of whole tissue proteomic data showing increased and decreased protein expression (cutoffs corresponding to a fold change >2 and a false discovery rate<0.05). Network visualization of increased and decreased gene ontologies in disease vs control tissue. Size corresponds with number of proteins involved in the node ($P \leq 0.05$, log fold change ≥2). **F**, NLRP3 ELISA conducted on whole tissue lysates normalized to 1 ug of whole tissue protein (*P=0.0360). **G**, Schematic representation of the domain organization of NLRP3, and residues identified in targeted mass spectrometry are noted with fragment ion m/z value denoted (*P=0.0130). Extracted ion chromatography AUC of all fragment ions shows significantly greater NLRP3 expression in disease vs control (nonparametric Mann–Whitney test). AUC indicates area under the curve; Ctrl, control; NLRP3, nucleotide oligomerization domain-like receptor family, pyrin domain containing 3; and PAD, peripheral arterial disease.

more atherogenic lesions seen in the control tissue. Notably, the presence of lipids determined by Oil Red O staining was markedly absent in both the disease and control tissues. CD68, used as a marker for the presence of macrophages, was markedly absent in the control tissue when compared with the disease tissue, with CD68-positive staining appearing to overlap with phagocytosis marker CD209 and NLRP3 staining in diseased tissue, which were absent in controls. Secreted inflammasome related-proteins IL-1β and caspase-1 showed faint staining in disease compared with control in adjusted regions to immunoreactive NLRP3 cells in serial sections. Transmission electron microscopy imaging demonstrated the presence of macrophage-like cells in proximity to calcific regions in PAD tissue, with smooth muscle cells appearing to be the more predominant cell type in control (Figure 2C and 2D). Immunofluorescent imaging demonstrated the colocalization of NLRP3 and CD68 in the presence and absence of calcification, denoted by near-infrared calcium tracer (Osteosense680) staining, which was visible in the PAD tissue and absent in control (Figure 2E and 2F). Less CD68-positive staining was present in the control tissue compared with PAD in the vascular wall, and NLRP3 colocalization (yellow) was not detected, suggesting a different cellular composition in PAD vessels compared with control, irrespective of calcification.

Proinflammatory Circulating Marker Expression Is Increased in Patients With PAD

Flow and ELISA-based analysis of PAD and control serum samples (Table S2) were used to confirm a systemic inflammatory profile in patients with PAD. NRLP3 protein levels in PAD (n=8) were significantly increased in comparison with control serum (n=6) (P=0.0007) (Figure 3A). Moreover, IL-1β was significantly increased in PAD serum compared with control (P=0.0127). Proinflammatory cytokines were assessed via a flow bead-based assay. PAD serum showed heterogeneity in the expression of present pro- and anti-inflammatory cytokines (Figure 3B). IL-6, IL-10, and IL-18, which support immunoregulation, were not significantly modulated in PAD compared with control. Notably, proinflammatory cytokines IL-23 (P=0.0589, r^2=0.2663) and IFNγ (interferon γ; P=0.0024, r^2=0.5495) were associated with donors who exhibited high levels of inflammation and high levels of calcification and NLRP3 activation. Moreover, IL-1β was increased relative to NLRP3 levels, with the highest IL-1β expression in the same patient, suggesting the association between NLRP3 and IL-1β in PAD.

DISCUSSION

With the growing burden of PAD set to become an epidemic in the United States and worldwide, there is a desperate need to identify mechanisms at play in PAD pathogenesis and progression,[3] with the ultimate goal to identify new therapeutic targets. The present study is the first to assess the whole-vessel proteomic signature of PAD tissue. Although the majority of proteins identified via proteomics were shared between both the control and PAD vessels, the abundance level of these proteins varied significantly, confirmed by the disparity in ontologies identified for differentially abundant proteins, notably highlighting a multitude of proinflammatory phenotypes. Proteomics analysis of PAD tissue demonstrated a reduction in extracellular matrix and structural organization,[10] contributing to vascular stiffening and producing a bed for calcification deposition in diseased vessels. Little is known about the role of the extracellular matrix in PAD beyond arterial stiffening or collagen enhancing the acquisition of macrophages to the area in atherosclerosis, with the current study giving further rationale for this to be investigated in more depth. Conversely, ontology signatures in proteins with increased abundance in PAD vessels highlighted the role of humoral immunity and acute inflammatory response, which is known to be.[11] Due to the role of NLRP3 in oxidative stress and inflammatory vascular environments, NLRP3 expression both in the circulating blood and peripheral vasculature was investigated. Increased NLRP3 was identified in vessels via targeted mass spectrometry and ELISA,

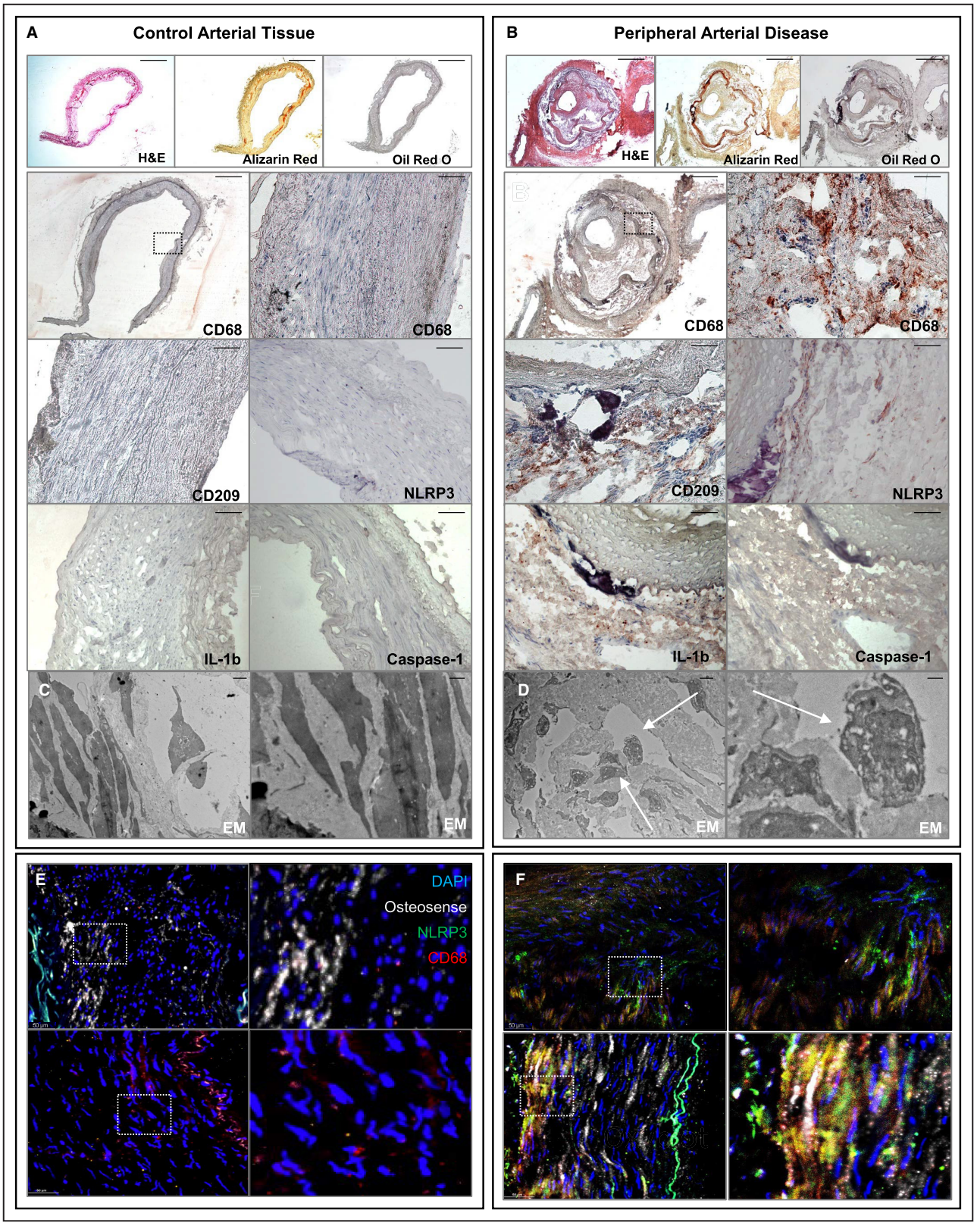

with colocalization staining demonstrating its presence in CD38-positive cells in the vicinity of calcification. The presence of CD68-positive, macrophage-like cells in calcific lesions has been evidenced previously,[9] but this study adds weight to the theory that there is inflammasome activation in CD68-positive cells adjacent

Figure 2. Histological analysis of peripheral arterial disease demonstrates NLRP3 presence in CD68-positive cells.
A and **B**, Alizarin Red, H&E, and Oil Red O staining. Alizarin Red staining appears more prominent in disease vs control, with H&E staining and nuclear staining more abundant in disease. Oil Red O staining shows little difference between the 2 conditions. CD68, CD209, NLRP3, IL-1β, and caspase-1 histological staining appears greater in disease compared with control tissue. **C** and **D**, Transmission electron microscopy images show the presence of macrophage-like cells adjacent to the calcified region, whereas smooth muscle cells appear the predominate cell-type in control tissue (magnifications ×2000 and ×8000). **E** and **F**, Immunofluorescent imaging of disease and control sections demonstrate greater NLRP3 staining in the disease compared with control (green). Colocalization of macrophage marker CD68 (red) and NLRP3 (green) appears yellow in insert (magnification ×2, scale bar=1000 μm; magnification ×20, scale bar=50 μm; magnification ×2000, scale bar=2 μm; magnification ×8000, scale bar = 500 nm). A, B, E and F, Black and white boxes (left panels) depict areas of low magnification for the adjacent images with high magnification (right panels). D, Arrows depict macrophage-like cells. CD68 indicates cluster of differentiation 68; CD209, cluster of differentiation 209; EM, electron microscopy; H&E, hematoxylin–eosin; IL-1β, interleukin 1β; and NLRP3, nucleotide oligomerization domain-like receptor family.

or in calcific regions in PAD, giving further rationale to the need to address PAD with anti-inflammatory therapeutics.

With inflammatory drivers, NLRP3, and its subsequent downstream markers IL-1β and caspase-1 identified in the local calcified vasculature, flow-based

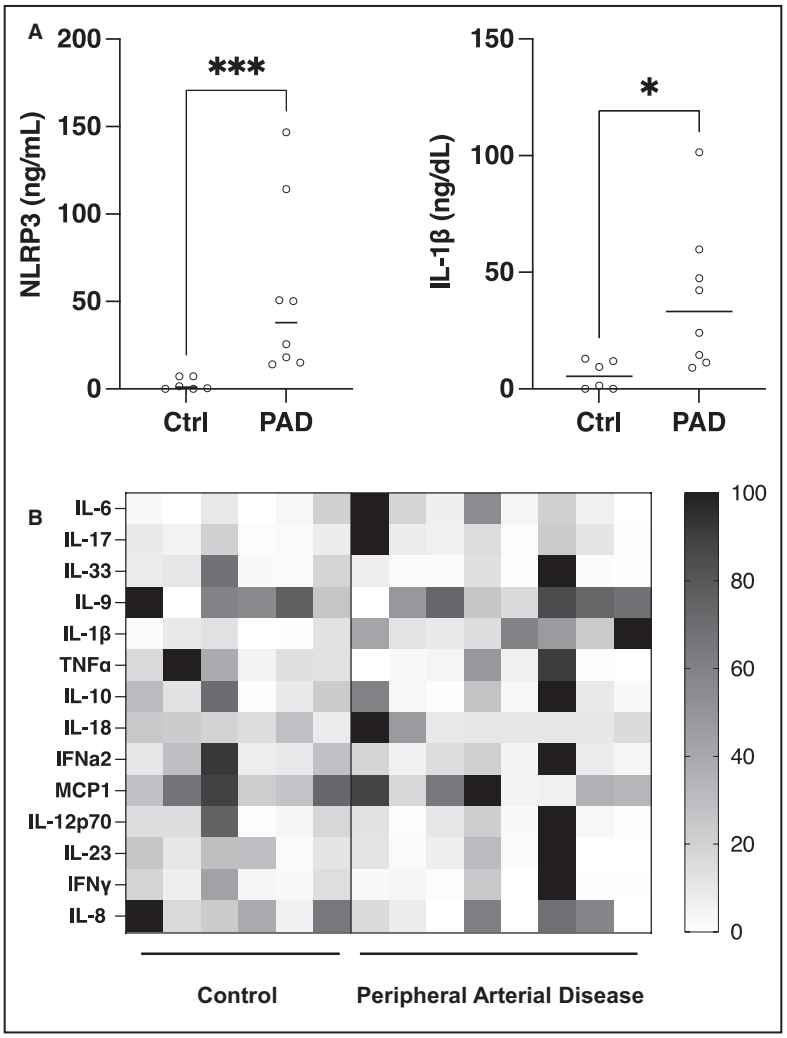

Figure 3. ELISA and flow-based analysis of PAD serum demonstrates heterogeneity in circulating proinflammatory markers and increased circulating NLRP3.
A, NLRP3 ELISA conducted on disease vs control serum. IL-1β assessed in serum via flow cytometric-based analysis showed significant increase in PAD vs control. **B**, Heatmap comparing the relative expression (0–100) of proinflammatory cytokines present in disease and control serum samples (nonparametric Mann–Whitney test, P=0.0007, P=0.0127). ***P<0.001, **P< 0.01 *P< 0.05. Ctrl indicates control; IFNγ, interferon γ; IL, interleukin; NLRP3, nucleotide oligomerization domain-like receptor family; PAD, peripheral arterial disease; and TNF-α, tumor necrosis factor α.

analysis was used to confirm a systemic circulatory inflammatory response in patients with PAD. Relative to control, increased IL-1β and elevated IL-17 and IL-23 further suggest the activation of NLRP3 at both local and systemic levels. As more studies give weight to the crucial role of inflammation in PAD, clinical trials have begun to investigate the inhibition of downstream inflammasome markers, specifically IL-1β and caspase-1, in pathologies associated with PAD and calcification, namely, type II diabetes and atherosclerosis.[6] In the data presented here, IL-1β was increased in PAD samples compared with control, suggesting the potential of repurposing of such drugs for patients with PAD. Notably, canakinumab, an IL-1β inhibitor, has been shown to reduce the recurrent rate of cardiovascular events[5] when compared with placebo. Because both local and systemic NLRP3 and associated cytokines were elevated in the current PAD cohort, further investigation should target the utility of these drugs. Similarity, AC-201, another IL-1β inhibitor, has been trialed in type II diabetes, with a reduction in HbA1c (hemoglobin A1c) shown, suggesting a primary role of inflammatory mediators and modulators central to disease pathogenesis. Conversely, however, a small, randomized trial of 38 participants with PAD treated with canakinumab had an increased number of serious adverse events (56% versus 50%) compared with the control, with no alternation of plaque progression in the superficial femoral artery.[4] Nevertheless, investigators observed an improvement in pain-free walking with canakinumab, with larger studies potentially underway, providing yet more impetus on the need to investigate anti-inflammatory lead treatment in PAD. Notably, basic research has also investigated the role of NLRP1 activation through PAD plasma in an in vitro endothelial model, and further research should be conducted to assess the synergy of these inflammasomes.[12] The primary limitation of this study is relatively small sample size, predominantly limited by the availability of non-diseased tissue, which may limit the ability to capture transiently activated pathways in relation to inflammation, and thus a larger study is required to fully elucidate these findings. Although the heterogeneity of calcification and localized inflammation in the vasculature has been reported,[13] this study is only a snapshot of a specific area of the vessel, which does not assess the global landscape. Future studies should seek to address these challenging technical issues.

In conclusion, these findings provide evidence of the presence of NLRP3 inflammasome in human PAD and a global proteomic profile of PAD tissue that was previously unreported. Moreover, the current results colocalize the presence of CD68-positive cells with NLRP3 and calcification in the vessels, thus providing mechanistic insight into the inflammatory mechanisms in PAD. Inhibition of the NLRP3 inflammasome activation or downstream signaling cascade may be beneficial to the reduction of inflammatory-driven PAD.

ARTICLE INFORMATION

Received June 19, 2022; accepted January 5, 2023.

Affiliations

Division of Cardiovascular Medicine, Department of Medicine, Center for Interdisciplinary Cardiovascular Sciences (F.B., J.Z., A.R.S., K.P., M.E.T., S.K., T.P., M.A., S.S., E.A.) and Division of Cardiovascular Medicine, Department of Medicine, Center for Excellence in Vascular Biology (A.R.S., M.A., E.A.), Brigham and Women's Hospital, Harvard Medical School, Boston, MA; Department of Surgery, Emory University School of MedicineAtlanta, GA (F.L., L.B.); and Surgical and Research Services Atlanta, Veterans Association Medical Centre, GA, Decatur (L.B.).

Sources of Funding

This work was supported by National Institutes of Health grants R01HL147095, R01HL141917, and R01HL136431 to Aikawa, American Heart Association institutional research grants 13IRG14740001 and R01HL143348 to Brewster, and a Boehringer Ingelheim Fonds MD fellowship to Zimmer.

Disclosures

Elena Aikawa serves on the Scientific Board for Elastrin Therapeutics.

Supplemental Material

Data S1
Tables S1–S5

REFERENCES

1. Polonsky TS, McDermott MM. Lower extremity peripheral artery disease without chronic limb-threatening ischemia: a review. *JAMA*. 2021;325:2188–2198. doi: 10.1001/jama.2021.2126
2. Aboyans V, Ricco JB, Bartelink MEL, Bjorck M, Brodmann M, Cohnert T, Collet JP, Czerny M, De Carlo M, Debus S, et al. 2017 ESC guidelines on the diagnosis and treatment of peripheral arterial diseases, in collaboration with the European Society for Vascular Surgery (ESVS): document covering atherosclerotic disease of extracranial carotid and vertebral, mesenteric, renal, upper and lower extremity arteries. Endorsed by: the European Stroke Organization (ESO) the Task Force for the Diagnosis and Treatment of Peripheral Arterial Diseases of the European Society of Cardiology (ESC) and of the European Society for Vascular Surgery (ESVS). *Eur Heart J*. 2018;39:763–816. doi: 10.1093/eurheartj/ehx095
3. Song P, Rudan D, Zhu Y, Fowkes FJI, Rahimi K, Fowkes FGR, Rudan I. Global, regional, and national prevalence and risk factors for peripheral artery disease in 2015: an updated systematic review and analysis. *Lancet Glob Health*. 2019;7:e1020–e1030. doi: 10.1016/s2214-109x(19)30255-4
4. Russell KS, Yates DP, Kramer CM, Feller A, Mahling P, Colin L, Clough T, Wang T, LaPerna L, Patel A, et al. A randomized, placebo-controlled trial of canakinumab in patients with peripheral artery disease. *Vasc Med*. 2019;24:414–421. doi: 10.1177/1358863x19859072
5. Ridker PM, Everett BM, Thuren T, MacFadyen JG, Chang WH, Ballantyne C, Fonseca F, Nicolau J, Koenig W, Anker SD, et al. Antiinflammatory therapy with canakinumab for atherosclerotic disease. *N Engl J Med*. 2017;377:1119–1131. doi: 10.1056/NEJMoa1707914
6. Wu D, Ren P, Zheng Y, Zhang L, Xu G, Xie W, Lloyd EE, Zhang S, Zhang Q, Curci JA, et al. NLRP3 (nucleotide oligomerization domain-like receptor family, pyrin domain containing 3)-caspase-1 Inflammasome degrades contractile proteins: implications for aortic biomechanical dysfunction and aneurysm and dissection formation. *Arterioscler Thromb Vasc Biol*. 2017;37:694–706. doi: 10.1161/atvbaha.116.307648
7. Hirsch AT, Criqui MH, Treat-Jacobson D, Regensteiner JG, Creager MA, Olin JW, Krook SH, Hunninghake DB, Comerota AJ, Walsh ME, et al. Peripheral arterial disease detection, awareness, and treatment in primary care. *JAMA*. 2001;286:1317–1324. doi: 10.1001/jama.286.11.1317
8. Lu J, Xie S, Deng Y, Xie X, Liu Y. Blocking the NLRP3 inflammasome reduces osteogenic calcification and M1 macrophage polarization

in a mouse model of calcified aortic valve stenosis. *Atherosclerosis*. 2022;347:28–38. doi: 10.1016/j.atherosclerosis.2022.03.005

9. Orecchioni M, Kobiyama K, Winkels H, Ghosheh Y, McArdle S, Mikulski Z, Kiosses WB, Fan Z, Wen L, Jung Y, et al. Olfactory receptor 2 in vascular macrophages drives atherosclerosis by NLRP3-dependent IL-1 production. *Science*. 2022;375:214–221. doi: 10.1126/science.abg3067
10. Hernández-Aguilera A, Nielsen SH, Bonache C, Fernández-Arroyo S, Martín-Paredero V, Fibla M, Karsdal MA, Genovese F, Menendez JA, Camps J, et al. Assessment of extracellular matrix-related biomarkers in patients with lower extremity artery disease. *J Vasc Surg*. 2018;68:1135–1142.e1136. doi: 10.1016/j.jvs.2017.12.071
11. Bartoli-Leonard F, Zimmer J, Aikawa E. Innate and adaptive immunity: the understudied driving force of heart valve disease. *Cardiovasc Res*. 2021;117:2506–2524. doi: 10.1093/cvr/cvab273
12. Bleda S, de Haro J, Varela C, Esparza L, Ferruelo A, Acin F. NLRP1 inflammasome, and not NLRP3, is the key in the shift to proinflammatory state on endothelial cells in peripheral arterial disease. *Int J Cardiol*. 2014;172:e282–e284. doi: 10.1016/j.ijcard.2013.12.201
13. Narula N, Dannenberg AJ, Olin JW, Bhatt DL, Johnson KW, Nadkarni G, Min J, Torii S, Poojary P, Anand SS, et al. Pathology of peripheral artery disease in patients with critical limb ischemia. *J Am Coll Cardiol*. 2018;72:2152–2163. doi: 10.1016/j.jacc.2018.08.002

SUPPLEMENTAL MATERIAL

Data S1

Supplemental Methods

Sample Collection

Human peripheral arteries (Table S1) were obtained from limb amputation surgeries (Emory University IRB #51432 and 70813) for participants either diagnosed with PAD or undergoing amputation for an unrelated reason, from a total of 14 donors (Table S1). No exclusion criteria were applied. Due to the difficulty in obtaining peripheral vessels, all available PAD and control vessels available were used. Samples were snap frozen in liquid nitrogen and stored in -80^{o}C until shipped to Brigham and Woman's Hospital for downstream analysis. Samples were then dissected on ice, with half used for proteomics and the other half for histology. Tissue samples were placed in 200uL of ice-cold RIPA buffer supplemented with protease and phosphatase inhibitor (Pierce, USA) for subsequent homogenization using a Precellys tissue homogenizer (Precelly lysing kit, Precellys, USA) using 3x 10 second cycles of 5000 RPM settings. Homogenates were then centrifuged (max. speed, 10 mins, 4^{o}C) and the supernatant used for downstream analysis. Serum samples were collected from PAD patients prior to surgery (Table S2). Control blood was purchased from 6 donors (Research Blood Components, USA). Serum was collected in BD vacutainer clot activator (BD#367812) tubes and stored at -80^{o}C prior to downstream analysis.

Histological Analysis

PAD tissue was embedded in OCT tissue freezing medium and frozen. 7 um fresh-frozen sections were cut via cryostat and fixed depending on stain. Sections for Oil Red O staining were fixed in 10% formalin for 5 minutes, before washing 3x in distilled water. Following air drying, slides were placed in absolute propylene glycol for 5 minutes and stained with pre-warmed Oil Red O solution for 10 minutes at 60^{o}C. Sections were differentiated in 85% propylene glycol solution for 5 minutes before rinsing 2x in distilled water. Sections were then counter-stained in Mayer's haematoxylin for 30 seconds and washed in water before mounting with aqueous mounting media. Sections for

Alizarin red staining were fixed in ice-cold acetone (100%) for 10 minutes at room temperature, before washing twice in PBS for 5 minutes. Slides were then submerged in 2% Alizarin red stain for 1 minute room temperature, before incubating with acetone (1 min), 50:50 acetone:xylene (1 min), xylene (1 min) and mounting with xylene-based mounting media. Sections were fixed in 4% PFA for 5 minutes, before haematoxylin and eosin staining conducted as previously described [9]. For immunohistochemical analysis sections were blocked with 0.3% hydrogen peroxidase (Fisher Scientific, USA) and incubated with 4% horse serum (Dako, USA). Primary antibodies (Table S3) were diluted in 4% horse serum and incubated for 90 minutes at room temperature in a humidified chamber and then incubated with biotinylated mouse or rabbit anti-goat secondary antibodies (Dako, USA). The streptavidin peroxidase method was used for each stain, and the reaction was visualised with a 3-amino-9-ethylcarbazol substrate (AEC substrate chromogen, Dako, USA). Sections were counter-stained with Gills Haematoxylin. All slides were imaged on a Nikon eclipse 50i.

Transmission Electron Microscopy

Fresh frozen sections were cut at 20 uM sections and placed in 4% PFA with 0.1% glutaraldehyde for 2 hours before placing in PBS supplemented with 20mM glycine and delivered to the Harvard Medical School Electron Microscopy Facility. Samples were then infiltrated with 2.3 M sucrose in PBS for 15 minutes and cut onto carbon coated copper grids before imaging by the core on an AMT camera system, HV=80.0kV, cal = 0.002 micron/pix.

Immunofluorescence

PAD sections were prepared as above. 7m fresh-frozen sections were cut via cryostat and fixed with 4% PFA for 10 minutes, washed 2x in PBS and blocked with 4% normal serum for 30 minutes. Sections were then incubated with primary antibodies (Table S3) for 1h at room temperature. Following washing 2x with PBS, sections were incubated with secondary antibodies for 30 minutes at room temperature. Sections were then washed as before and incubated with

DAPI (4', 6-Diamidino-2-Phenylindole, Dihydrochloride, Thermo, USA) for nuclear counter staining. Sections were imaged using confocal microscopy on a Nikon confocal A1 microscope.

NLRP3 ELISA

Human NLRP3 SimpleStep ELISA (ab27401, Abcam, USA) was run following manufacturer's instructions. Briefly, 50 uL of standards and 50 uL of 1:10 diluted tissue samples and 1:1 serum diluted samples were loaded in duplicate. Following 1 hour of incubation with 50 uL antibody cocktail all wells were washed 3x in wash buffer and developed with 100 uL of TMB development solution for 10 minutes. Finally, 100 uL of stop solution was then added and the plate read at OD 450nm on a spectramax 3 (Molecular probes, USA).

Tissue Proteolysis

Homogenized human peripheral vessels samples were proteolyzed using the iST in-solution digestion kit (PreOmics, USA) automated on the PreON robot (PreOmics, USA). Briefly, 50ug of protein was lysed with 50 uL LYSE buffer and heated to 95^{o}C for 10 minutes. Samples were digested for 2 hours following manufacturer's instructions. Eluted peptides were then dried via speed vacuum (Eppendorf Vacufuge) and resuspended in 40 uL in LC-LOAD. 4 uL of 1:20 diluted peptide stock (250 ng protein stock) was analysed via mass spectrometry.

Mass Spectrometry

Data-dependent acquisition (DDA) mass spectrometry was acquired on the Orbitrap Fusion Lumos coupled to a heated EASY-spray nanosource and nanoLC1000 (Thermo Fisher Scientific, USA). Peptides were first subjected to an Acclaim PepMap RSLC C18 trap column and then separated with a heated EASY-Spray column (Thermo Fisher Scientific). The analytical gradient was run at 300 nl/min from 5 to 21% Solvent B (acetonitrile/0.1% formic acid) for 75 minutes, 21 to 30% Solvent B for 10 minutes, followed by 10 minutes of 95% Solvent B. Solvent A was water/0.1% formic acid. Acetonitrile and water were LC-MS-grade. Analytical gradient was run at 300 nl/min from 5 to 21% Solvent B (acetonitrile/0.1% formic acid) for 75 minutes, 21 to 30%

Solvent B for 10 minutes, followed by a 95% to 5% Solvent B jigsaw wash. Solvent A was water/0.1% formic acid. Acetonitrile and water were LC-MS-grade. The Orbitrap was set to 120 K resolution, and the top N precursor ions in 3 seconds cycle time within a scan range of m/z 400-1500 (60 sec dynamic exclusion) were subjected to collision induced dissociation (CID; collision energy, 30%; isolation window, 1.6 m/z). The ion trap was set to a rapid scan rate for peptide sequencing (MS/MS).

Mass Spectral Analysis

DDA spectra collected from the scan range of m/z 400-1500 were queried against the human UniProt database (downloaded September 2020; 96, 816 entries) with the HT-SEQUEST search algorithm, via Proteome Discover 2.2 (Thermo Fisher Scientific) using a 10 ppm tolerance window in MS1 and a 0.6 Da fragment tolerance window for MS2; trypsin as the protease with carbamidomethylation as a static modification and oxidation of methionine as variable modification. The peptide false discovery rate of 1% was calculated using Percolator within Proteome Discover (PD). Peptides assigned to a given protein group, and not present in any other protein group, were considered as unique. Consequently, each protein group is represented by a single master protein (PD Grouping feature). Unique and razor peptides were used per protein for quantification. Quantification of proteins across samples (the 14 vessel samples) was completed via Feature Mapper. Chromatographic alignment, the maximum retention shift was 10 minutes and mass tolerance of 10 ppm. Precursor peptide abundances were based on their chromatographic intensities and total peptide amount was used for normalization. Proteins used for downstream quantification were filtered by having 2 or more unique peptides. Magnitude of missing values was 10.69% of total proteins identified. The final protein list is therefore a consensus proteome of the 14 vessels. Proteome Discover results were normalised by the protein median before downstream analysis via an inhouse script.

NLRP3 Targeted Mass Spectrometry

1 ug NLRP3 (H00114548, Novus Biologicals, USA) was proteolyzed as above and analysed by the Lumos using a shorter analytical gradient: 300 nl/min from 8 to 25% Solvent B for 20 minutes, 25 to 35% Solvent B for 5 minutes, followed by the jigsaw wash. The Orbitrap was set to 120 K resolution, and the top N precursor ions in 3 seconds cycle time within a scan range of m/z 400-1500 (30 sec dynamic exclusion) were subjected to higher energy collision induced dissociation (HCD; collision energy, 30%; isolation window, 1.2 m/z; 30 K resolution) for MS/MS. The most abundant NLRP3 peptide (Table S5), as identified using Proteome Discoverer, was monitored in the 14 vessel samples. The peptide was monitored using the targeted MS2 module acquired in profile mode: precursor isolation window, 0.8 m/z; collision energy, 30%, scan range, m/z 350-1200; resolution, 240 K. The extracted ion chromatogram of each fragment ion's monoisotopic peak was quantified using QualBrowser (Thermo Fisher Scientific).

Differential Enrichment and Gene Ontology Analysis

Differentially abundant proteins between PAD and control were identified using *limma* 3.46 [10] in R using whole tissue proteomics. Briefly, limma uses lmFit() and eBayes() to estimate the variance by exchanging information between genes for reducing false positives and detect genes with large variance (logFC<2 and adjusted p-value (Benjamini-Hochberg) < 0.05). The differential abundant proteins list was then analysed for enriched pathways using clusterProfiler 3.18 [11] in R using function enrichGO. The ontologies were plotted using cnetplot().

Multi-Analyte LegendPlex Flow Assay

Human Inflammation panel 1 and a custom LegendPlex panel (containing IL-6, IL-18, IL-9 and IL-1β) (Cat. 740809 & 900001042 Biolegend, USA) was conducted following manufacturer's instructions. Briefly, serum samples were diluted 2-fold with assay buffer before use. 25 uL of diluted sample was incubated with 25 uL of assay buffer and 25 uL of standards were incubated with 25 uL Matrix B3 and B1 respectively. 25 uL of human inflammation panel 1 premixed beads were added and the plate was shaken at 800 rpm for 2 hours at room temperature. The plate was then centrifuged and supernatant removed and the beads were washed twice with 200uL 1x wash

buffer. 25 uL of detection antibodies were then added and shaken at 800 rpm for 1 hour at room temperature. Subsequently 25 uL of Streptavidin, R-Phycoerythrin (SA-PE) was added directly to each well and shaken at 800 rpm for 30 minutes at room temperature. Wells were then washed again as before, and beads resuspended in 150uL wash buffer and assessed immediately on the Cytek Aurora, (Cytek, USA).

Statistical Analysis

Graphpad Prism (V9.0) and R (V4.2) was used to analyse data. Non-parametric tests such as Wilcoxon test were conducted on non-normally distributed data. Association of NLRP3 and cytokines was conducted via linear regression on Graphpad Prism. Graphs were produced in Prism and R. Proteomic data exploration was conducted using Qlucore Omics Explorer 3.2 (Qlucore, Sweden).

Table S1. Patient Tissue Demographics.

ID	PAD	Age	Sex	Diabetes	Dyslipidemia	Smoking	Chronic I	Indication	Sample
#2	Y	60	M	Y	N	N	N	Infection	Peroneal artery
#3	Y	32	M	N	N	N	Y	Infection	Tibial artery
#4	Y	76	M	N	Y	Y	N	Ischemic	Popliteal artery
#5	Y	76	F	Y	N	N	N	Infection	Peroneal artery
#8	Y	67	F	Y	Y	N	N	Ischemic	Tibial artery
#9	Y	46	M	N	N	N	N	Ischemic	Popliteal artery
#12	Y	81	F	N	N	N	N	Ischemic	Tibial artery
#19	Y	66	M	Y	N	N	Y	Ischemic	Peroneal artery
#28	Y	66	M	Y	N	N	Y	Infection	Tibial artery
#29	Y	59	M	Y	N	N	N	Ischemic	Peroneal artery
#33	N	29	M	N	N	N	N	Control	Tibial artery
#77	N	67	F	Y	N	N	N	Control	Tibial artery
#107	N	67	M	N	N	N	N	Control	Peroneal artery
#108	N	74	M	N	N	N	N	control	Peroneal artery

Table S2. Patient serum demographics.

ID	PAD	Age	Sex	Diabetes	Dyslipidemia	Smoking	Chronic Kidney Disease	Indication	Sample
01-0043	Y	43	M	Y	N	N	Y, ESRD	PAD	Serum
01-0047	Y	77	M	Y	N	N	N	PAD	Serum
01-0051	Y	75	F	N	Y	N	N	PAD	Serum
01-0065	Y	70	M	N	Y	Y	N	PAD	Serum
01-0066	Y	62	M	Y	Y	N	N	PAD	Serum
01-0070	Y	68	M	N	N	N	N	PAD	Serum
01-0072	Y	64	F	Y	N	Y	N	PAD	Serum
01-0080	Y	54	F	N	N	N	N	PAD	Serum
1-64379	N	55	F	N	N	N	N	Control	Serum
2-64373	N	38	M	N	N	N	N	Control	Serum
3-64372	N	55	M	N	N	N	N	Control	Serum
4-64375	N	34	M	N	N	N	N	Control	Serum
5-64377	N	45	M	N	N	N	N	Control	Serum
6-64374	N	56	M	N	N	N	N	Control	Serum

Table S3. Antibodies Used.

Epitope	Supplier	Catalog No.	Dilution	Use
CD68	Abcam	ab213363	1:200	IHC
CD209	Abcam	Ab245200	1:200	IHC
NLRP3	Novus Biologics	NBP2-12446	1:100	IHC
Caspase 1	Cell Signalling Technology	D57A2	1:500	IHC
IL-1 beta	Cell Signalling Technology	12703	1:500	IHC
NLRP3	Novus Biologics	NBP2-12446	1:200	ICC
CD68	Abcam	ab213363	1:500	ICC

Table S4. NLRP3 Peptide Library.

NLRP3 peptide	RT start (min)	RT end (min)	Precursor m/z	Precursor charge	Fragment ion	Fragment ion m/z
GDILLSSLIR	22.5	26	543.83	2	y6	688.435
GDILLSSLIR	22.5	26	543.83	2	y5	575.351
GDILLSSLIR	22.5	26	543.83	2	y7	801.516

Table S5. Gene Ontology Input for Networks. See Excel file.